Published in final edited form as:

Clin Cancer Res. 2017 August 01; 23(15): 4335–4346. doi:10.1158/1078-0432.CCR-16-2955.

Radium-223 inhibits osseous prostate cancer growth by dual targeting of cancer cells and bone microenvironment in mouse models

Mari I. Suominen[1], **Katja M. Fagerlund**[1], **Jukka P. Rissanen**[1,7], **Yvonne M. Konkol**[1,8], **Jukka P. Morko**[1], **ZhiQi Peng**[1], **Esa J. Alhoniemi**[2], **Salla K. Laine**[3], **Eva Corey**[4], **Dominik Mumberg**[5], **Karl Ziegelbauer**[5], **Sanna-Maria Käkönen**[3,6], **Jussi M. Halleen**[1], **Robert L. Vessella**[4], and **Arne Scholz**[5]

[1]Pharmatest Services Ltd., Turku, Finland [2]Avoltus Oy, Turku, Finland [3]Aurexel Life Sciences Ltd., Askainen, Finland [4]Department of Urology, University of Washington, Seattle, WA, USA [5]Bayer AG, Pharmaceuticals Division, Drug Discovery, Therapeutic Research Groups Oncology, Berlin, Germany [6]Department of Cell Biology and Anatomy, University of Turku, Turku, Finland

Abstract

Purpose—Radium-223 dichloride (radium-223, Xofigo®), a targeted alpha therapy, is currently used for the treatment of patients with castration-resistant prostate cancer (CRPC) with bone metastases. This study examines the mode-of-action and antitumor efficacy of radium-223 in two prostate cancer xenograft models.

Experimental Design—Mice bearing intratibial LNCaP or LuCaP 58 tumors were randomized to groups (n = 12–17) based on lesion grade and/or serum PSA level and administered with radium-223 (300 kBq/kg) or vehicle, twice at 4-week intervals. X-rays and serum samples were obtained biweekly. Soft tissue tumors were observed macroscopically at sacrifice. Tibiae were analyzed by gamma counter, micro-CT, autoradiography and histology.

Results—Radium-223 inhibited tumor-induced osteoblastic bone growth and protected normal bone architecture leading to reduced bone volume in LNCaP and abiraterone-resistant LuCaP 58 models. Furthermore, radium-223 resulted in lower PSA values and reduced total tissue and tumor areas, indicating that treatment constrains prostate cancer growth in bone. In addition, radium-223 suppressed abnormal bone metabolic activity as evidenced by decreased number of osteoblasts and osteoclasts and reduced level of the bone formation marker PINP. Mode-of-action studies revealed that radium-223 was deposited in the intratumoral bone matrix. DNA double-strand breaks were induced in cancer cells within 24 hours after radium-223 treatment and PSA levels were significantly lower 72 hours post treatment providing further evidence of the anti-tumor effects.

Corresponding Author: Arne Scholz, MD, Bayer AG, Pharmaceuticals Division, Drug Discovery, Therapeutic Research Groups Oncology II, Müllerstr. 178, 13353, Berlin, Germany; arne.scholz@bayer.com.
[7]Present affiliation: Preclinapps Ltd., Raisio, Finland
[8]Present affiliation: Department of Cell Biology and Anatomy, University of Turku, Turku, Finland

Conclusion—Taken together, radium-223 therapy exhibits a dual targeting mode-of-action that induces tumor cell death and suppresses tumor-induced pathological bone formation in tumor microenvironment in osseous CRPC growth in mice.

Keywords

radium-223; prostate; bone metastases; CRPC; abiraterone resistance

Introduction

Prostate cancer is the second most frequently diagnosed cancer worldwide and the third leading cause of cancer-related mortality in men in developed countries (1). While surgery and radiation therapy offer effective treatment against localized prostate cancer, curative options for metastatic prostate cancer remain elusive. Hormone ablation therapy represents the most common therapeutic option for locally advanced or widespread prostate cancer. However, most patients eventually develop resistance to androgen deprivation therapy and progress towards the terminal stage of the disease, castration-resistant prostate cancer (CRPC). In addition to the treatment resistance, the risk of developing metastatic bone disease secondary to prostate cancer, and increased bone loss due to androgen deprivation therapy represent significant clinical obstacles in the treatment of patients with advanced prostate cancer (2).

Bone metastases accompanying prostate cancer feature a state of accelerated bone turnover with abnormal activation of both osteoclasts and osteoblasts, and consequent abnormal bone formation, resulting in fragile, disorganized woven bone (2). This leads to increased risk of skeletal fractures, immobility, severe bone pain, a significant decrease in quality of life, increased mortality and, consequently, remarkable economic burden (3, 4). Therefore, the elimination of cancer in bone and the restoration and/or preservation of healthy bone morphology are important goals in the management and treatment of prostate cancer.

Abiraterone (cytochrome P (CYP17) inhibitor) and enzalutamide (androgen receptor inhibitor) have been approved by the FDA and the European Medicines Agency (EMA) for the treatment of patients with CRPC. Although these secondary androgen suppression agents show high efficacy in Phase III trials (5–8), their impact on bone microenvironment remains largely unknown. One report has suggested that CYP17 inhibition with abiraterone has direct effects on bone anabolic and anti-resorptive activity (9).

Radium-223 dichloride (radium-223, Xofigo®) is the first targeted alpha-therapy approved by FDA and EMA for the treatment of patients with CRPC with symptomatic bone metastases and no known visceral metastatic disease. It is an alpha particle (α)-emitting calcium-mimetic that selectively binds to hydroxyapatite in the bone, targets areas of increased bone turnover such as osteoblastic bone metastases and improves the median overall survival in a large phase III trial in patients with CRPC and bone metastases (10). In addition, radium-223 has also been shown to significantly delay the manifestation of the first clinically identified symptomatic skeletal events (SSE) (11).

In a mouse model of osteolytic breast cancer bone metastasis, radium-223 reduced development of osteolytic lesions and improved survival by inducing DNA double-strand breaks in tumor cells and decreasing the number of osteoclasts (12). Whether radium-223 impact on CRPC bone metastasis occurs via a similar mechanism has not been investigated yet. Here, we exploited two mouse models of osteoblastic reaction resulting from prostate cancer growth in the bone environment mimicking the devastating bone disease observed in prostate cancer patients to investigate the efficacy and mode-of-action of radium-223.

Materials and methods

Compounds

Radium-223 was synthesized at Institute for Energy and Technology (Norway) as a solution containing 60 kBq/ml of radium-223 dichloride. Abiraterone acetate (abiraterone, Zytiga®) was obtained from Janssen Biotech (Horsham, PA, USA).

Cells

LNCaP cells were purchased from ATCC (November 2013) and maintained in standard cell culture conditions as indicated by provider for three months until the experiment was started. Cells were authenticated in June 2014 using short tandem repeat analysis (GenePrint10 system, Promega, Madison, WI, USA) at Institute for Molecular Medicine Finland (FIMM, Helsinki, Finland). LuCaP 58 patient-derived xenograft (PDX) was licensed from the University of Washington (13) and propagated subcutaneously in intact male SCID mice (CB17/*lcr-Prkdc*^{scid}/*lcrCrl*, Charles River, Germany) until the experiment was started (July 2013). LuCaP 58 tumors were demonstrated as *Mycoplasma* free in January 2013 using IDEXX PCR test (IDEXX, Columbia, MI, USA). For intratibial inoculation, tumors were harvested and processed to single cell suspension as described before (13). Briefly, the cells were mechanically dissociated and placed in Hank's balanced salt solution (HBSS, Lonza, Basel, Switzerland). Red blood cells were lysed with a solution containing 0.15 M NH_4Cl, 0.01 M $NaHCO_3$ and 0.09 mM EDTA using 5:1 (vol:vol) ratio at room temperature, and the reaction was stopped with three-fold volume of HBSS. The cell suspension was washed at least two times with PBS. The viability of the cell suspension was ~20%.

In vivo models

All experiments were approved by the Animal Experiment Board of Finland and performed according to guidelines of the European Union directive 2010/63/EU. Mice were kept under pathogen-free and controlled conditions and fed 2916 Teklad Global diet (Harlan Laboratories, B.V., Horst, the Netherlands). The effects of radium-223 were studied in cell line-based LNCaP and patient-derived LuCaP 58 prostate cancer xenograft models in mice. With LuCaP 58 mice, three individual studies were carried out to assess the efficacy and mode-of-action of radium-223 as well as sensitivity for abiraterone. The administration dose of 300 kBq/kg was selected based on a previous dose-escalation study in mouse model of breast cancer bone metastasis, representing 12% of the severely toxic dose of radium-223 to 10% of the mice (STD10) after single administration. (12). For the cell line-based model, LNCaP cells (2×10^6 cells in 20 μl of PBS) were inoculated into the right proximal tibia of 7-week-old male NOD SCID mice (NOD.CB17-*Prkdc*^{scid}/NcrCrl, Charles River, Germany).

The mice were anesthetized via isoflurane inhalation (IsoFlo vet, Abbot Laboratories, Berkshire, UK). Analgesia was provided with buprenorphine (0.3 mg/ml Temgesic®, RB Pharmaceuticals Ltd., Berkshire, UK) once before the intratibial inoculation (0.1 mg/kg, s.c.), and for 2 days after the intratibial inoculation and for the last 5 days of the experiment (0.02 mg/ml in drinking water). After 6 weeks, mice with tumor-induced osteoblastic, mixed and osteolytic changes as observed by radiography were randomized into two groups (n = 13–14 per group) based on lesion score (1–3) and serum prostate-specific antigen (PSA) value prior to treatment. Radium-223 (300 kBq/kg) and vehicle (28 mmol/L sodium citrate, Institute for Energy Technology, Norway) were administered intravenously (i.v.) one day after randomization, and at 4 weeks after first dose, followed by sacrifice 6 weeks after the first dose.

Blood samples were collected from the saphenous vein 6 weeks after LNCaP tumor cell inoculation and biweekly thereafter and additionally by cardiac puncture at sacrifice. Body weight was measured twice weekly. Tumors in soft tissues, including liver, adrenal glands, heart, lungs and pancreas, were observed macroscopically at sacrifice. The tumor-bearing and contralateral healthy tibiae were collected, weighed and measured for radium-223 activity using a gamma counter (1260 Multigamma II, LKB/Wallac, Turku, Finland). Serum PSA levels were analyzed using Quantikine Human Kallikrein 3/PSA enzyme-linked immunosorbent assay (ELISA) kit (R&D Systems, Minneapolis, MN, USA) and N-terminal propeptide of type I procollagen (PINP) concentration was determined using Rat/Mouse PINP enzymeimmunoassay (EIA) kit (IDS Ltd, Boldon, UK). Mice were sacrificed with CO_2 followed by cervical dislocation.

For the PDX model, LuCaP 58 cells as single-cell suspension of $1x10^6$ cells in 20 µl of PBS harvested from subcutaneous tumors were inoculated into the bone marrow cavity of tibia of SCID mice (Charles River, Germany and Harlan, Italy). Mice with apparent bone changes at 7 or 9 weeks after tumor inoculation were selected for the study. Blood samples were collected at 3 weeks after cell inoculation, and biweekly thereafter as described above. To assess the efficacy, animals were randomized into two groups (n = 15–17 per group) based on serum PSA levels; the first mice reached the inclusion criteria (PSA > 1 ng/mL) at 7 weeks and the rest at 9 weeks after tumor inoculation. Radium-223 (300 kBq/kg) and 28 mmol/L sodium citrate (vehicle) were administered intravenously (i.v.) on the first day after randomization and 4 weeks later, followed by sacrifice 6 weeks after the first dose, or earlier if weight loss exceeded 20%.

In the mode-of-action study, LuCaP 58 mice were randomized into groups (n = 12 per group) based on PSA level at 7 weeks after tumor inoculation. Radium-223 (300 kBq/kg) was administered as a single dose, followed by sacrifice at 24, 48, or 72 h. Mice in the vehicle group were sacrificed at 72 h.

For comparison of the efficacy between radium-223 and abiraterone in LuCaP 58 PDX model, mice were randomized (n = 17 per group) based on serum PSA levels and administered with vehicle (28 mmol/L sodium citrate for radium-223 and 5% benzyl benzoate in 95% peanut oil for abiraterone) radium-223 (300 kBq/kg, i.v., on the first day

after randomization and 4 weeks later) or abiraterone (daily, 200 mg/kg, p.o.), followed by sacrifice 6 weeks after the first dose.

Histology, histomorphometry and autoradiography

Tibiae were fixed in 4% PFA (paraformaldehyde) for 1–2 days, decalcified in 14% EDTA for two weeks, processed to paraffin blocks and then cut to 4 μm sections. Tumor and bone areas were measured from mid-sagittal sections of each tibia stained with haematoxylin-eosin (HE) (Harris haematoxylin, CellPath) or Masson-Goldner Trichrome (MGT), using MetaMorph image analysis software (Molecular Devices, LLC, Sunnyvale, CA).

Multinucleated (>1 nuclei) osteoclasts in the tumor-bone interface were counted in TRACP (tartrate-resistant acid phosphatase)–stained sections and normalized to the length of the tumor-bone interface. Whole section was analyzed. Osteoblasts were counted from MGT-stained sections based on morphology and location. Two microscope fields at 10x magnification were analyzed.

The effect of radium-223 on inducing DNA double-strand breaks was evaluated by immunohistochemical staining of g-H2AX molecules (JBW301, Millipore) as previously described (14). Four microscope fields (when possible) were counted for g-H2AX positive tumor cells using 40x objective. g-H2AX positive osteoblasts and multinucleated osteoclasts on bone were counted in TRACP and g-H2AX-doublestained sections. Samples (n = 6 per group) were obtained from mice sacrificed at 24, 48, or 72 h after radium-223 administration, and analyzed in one mid-sagittal section per sample using Leica DM4000 B Research Microscope (Leica Microsystems, Wetzlar, Germany).

For autoradiography, undecalcified tibiae (n = 6 per group) from radium-223-treated mice sacrificed at 24, 48 or 72 h post dosing were embedded in methyl methacrylate, cut to 4 μm thick sections and after plastic removal dipped in Ilford K5 emulsion (Polysciences Inc., Warrington, PA, USA). Sections were then held in a light-protected box for 3 days at room temperature, processed according to manufacturer’s instructions and counterstained with MGT staining.

Radiographic and micro-CT imaging

Radiography was performed at two weeks and at sacrifice (days 22–25) and micro-CT imaging at sacrifice. For radiography, the animals were anesthetized by inhalation of isoflurane and x-rayed in an anteroposterior position using the Faxitron Specimen Radiographic System MX-20 D12 (Faxitron Corp., Illinois, USA) with Faxitron Dicom 3.0– software. Minimum of two radiographs (both hind limbs) per animal were taken at each analysis point (34 kV, 7 seconds, 2-fold magnification). The formation of tumor-induced osteoblastic, mixed and osteolytic changes in bone (lesion area) was determined from the images with the MetaMorph software. Micro-CT measurements on the fixed tibias were performed using SkyScan 1072 scanner (Bruker, Kontich, Belgium) using voxel size of 7 μm. The measurement region was 6 mm wide, starting from 0.2 mm below the growth plate and the lower threshold for total bone intensity was 80. Trabecular and cortical bone could not be analyzed separately due to the massive destruction of normal bone architecture in the control group. Thus, only total bone was analyzed with lower intensity threshold of 80.

Statistical methods

Statistical analysis was performed with statistical software R (15) (version 3.1.0 or newer). All statistical analyses were performed as two-sided tests. For end-point analyses, data normality and homogeneity of variance were evaluated before further analyses. In the case of violating these assumptions, either log or other appropriate transformation (e.g. square root, reciprocal) was applied. If the assumptions were fulfilled as such or after a transformation, the group comparisons were carried out using one-way ANOVA followed by Tukey's HSD post hoc test (in the case of statistically significant ANOVA; $p < 0.05$). If the assumptions were not fulfilled, Kruskal-Wallis test followed by Mann-Whitney U test for pairwise comparisons (in the case of significant Kruskal-Wallis test; $p < 0.05$) were used. If an analysis contained only one comparison, either Student's t test (normally distributed data) or Mann-Whitney U test (non-normal data) was applied. For the analysis of the proportion of animals with visceral metastases, Fischer's exact test was used. The parameters assessed in multiple time points as well as total activities between control and tumor-bearing tibiae were analyzed using either fixed or mixed models (estimated using R package nlme (16). The hypotheses (e.g. comparisons between two groups at specific time points) were tested using model contrasts. In the case of multiple comparisons, the p-values were adjusted to avoid false positives. Contrasts and the corresponding p-values were computed using R package multcomp (17).

Results

Radium-223 inhibits tumor growth in prostate cancer mouse models

The effects of radium-223 on tumor growth were investigated in LNCaP cell line and LuCaP 58 patient-derived xenograft models in mice (Supplementary Table S1). Serum PSA levels and lesion areas (osteoblastic, mixed and osteolytic changes in bone determined using radiography) were measured biweekly and tumor growth was evaluated histologically. Mice treated with radium-223 (300 kBq/kg, twice with 4-week interval) exhibited lower serum PSA levels in comparison to vehicle control (LNCaP, $p = 0.02771$; LuCaP 58, $p = 0.00191$) (Fig. 1A–B). Despite the clear reduction compared to control, PSA level remained stable or increased during time course in radium-223-treated LNCaP and LuCaP 58 xenografts, respectively, similar to clinical observations (18, 19). Histological evaluation of tumor-bearing tibiae at sacrifice revealed reduced tumor area (LNCaP, $p = 0.00928$, 68% reduction; LuCaP 58, $p = 0.09817$, 25% reduction), total tissue area (consisting of bone, bone marrow and tumor) (LNCaP, $p = 0.00076$, 16% reduction; LuCaP 58, $p = 0.00655$, 26% reduction), and tumor-bone interface (LNCaP, $p = 0.00122$, 82% reduction; LuCaP 58, $p = 0.00014$) in radium-223-treated mice as compared to vehicle control (Fig. 1C–H). In LuCaP 58 mice, the reduction in tumor area was not statistically significant. This difference may be due to the fact that the LuCaP 58 tumor was growing more aggressively than LNCaP, as indicated by a 5-fold higher average tumor area in LuCaP 58 mice compared to LNCaP. Furthermore, the proportion of bone marrow occupied by tumor cells (not including area of tumor-induced bone) was decreased in radium-223-treated LNCaP xenografts, while in LuCaP 58 xenografts no difference was observed (LNCaP, $p = 0.02486$, 57% decrease; LuCaP 58, $p = 0.72855$, 2% decrease) presumably due to more aggressive tumor growth. In addition, the weight of tumor-bearing tibiae at sacrifice was decreased in LuCaP 58 xenografts in

response to radium-223 treatment (38% decrease; p = 0.02697). Taken together, these data indicate that radium-223 inhibits tumor growth on both LNCaP and LuCaP 58 tumors.

Radium-223 inhibits tumor-induced bone formation in both LNCaP and LuCaP 58 xenograft models

Prostate cancer growth in bone associated SREs are caused by pathological and structurally weak bone resulting from abnormal activation of both osteoclasts and osteoblasts by prostate cancer. To better understand the role of radium-223 in preventing the SREs, the effects of radium-223 on bone were investigated in LNCaP and LuCaP 58 xenograft models. In both models, mice administered with radium-223 at 300 kBq/kg, twice with 4-week interval, exhibited significantly reduced bone volume (LNCaP, p = 0.00450, 17% reduction; LuCaP 58, p < 0.001, 28% reduction), bone surface area (LNCaP, p < 0.001, 22% reduction; LuCaP 58, p < 0.001, 45% reduction), and bone surface density (LNCaP, p < 0.001, 21% reduction; LuCaP 58, p < 0.001, 30% reduction) in tumor-bearing tibias in comparison to vehicle control, as measured by micro-CT (Fig. 2A–D). The lesion area consisting of mainly osteoblastic, but also mixed and osteolytic tumor-induced pathological changes as observed by radiography was decreased in both LNCaP (p = 0.00366) and LuCaP 58 (p = 0.01702) tumor-bearing tibiae (Fig. 2E–H). In addition, radium-223 treatment resulted in lower levels of bone formation biomarker PINP in LNCaP (p < 0.001) and LuCaP 58 (p = 0.00548) models in comparison to untreated animals (Fig. 2I–J). These results indicate that radium-223 suppresses the abnormal bone formation in tumor microenvironment.

The beneficial effect of radium-223 on tumor-induced pathological bone effects was further supported by histomorphometry of LNCaP and LuCaP 58 tumor-bearing tibiae showing markedly reduced total bone area (LNCaP, p < 0.00059, 16% reduction; LuCaP 58, p = 0.059, 30% reduction) and relative trabecular bone area (LNCaP, p = 0.00564, 12% reduction; LuCaP 58, p = 0.0212, 56% reduction) in LNCaP and LuCaP 58 models in comparison to vehicle control (Fig. 3A–E). Similarly to tumor area, the reduction in total bone area was not significant in LuCaP 58 model. Histological analyses revealed that tibias were filled with LuCaP 58 tumor and additional ectopic tumor growth was observed (Fig. 3A–B), resulting in higher total tissue area in these mice compared to LNCaP xenografts (Fig. 1E–F). With regard to bone cells, radium-223 reduced the number of osteoblasts relative to bone surface in histologic sections of bone metastases in both models (Fig. 3F–G; LNCaP, p = 0.00127, 90% reduction; LuCaP 58, p = 0.0014, 77% reduction) and a total eradication of osteoclasts at tumor-bone interface was observed in LNCaP model (p = 0.01207) in response to radium-223 therapy. In contrast, in LuCaP 58 xenografts no difference was observed (p = 0.19644) in the number of osteoclasts relative to tumor-bone interface in response to radium-223 therapy (Fig. 3H–I), although the tumor-bone interface length and thus also the absolute number of osteoclasts at tumor-bone interface was decreased (p = 0.00106, 61% reduction). Taken together, these data demonstrate that radium-223 decreases the tumor-induced pathological bone formation by suppressing the accelerated bone turnover in tumor-bearing tibias.

Interestingly, unlike radium-223, abiraterone treatment was not able to reduce tumor growth or pathological bone changes in intratibial LuCaP 58 PDX model (Supplementary Fig. S1,

Supplementary Table S2), suggesting that radium-223 could be a potential option for patients with acquired abiraterone resistance.

Visceral metastases in radium-223-treated mice

To evaluate the effect of radium-223 in the development of metastases in soft tissue, mice bearing LuCaP 58 cells were macroscopically evaluated for visceral metastases. The number of mice affected by visceral spread was lower in the radium-223 treatment group; however, the differences were not statistically significant (Fig. 4). In mice bearing LNCaP cells, tumor growth was not observed in other sites than in the inoculated tibiae.

Radium-223 is deposited in the intratumoral bone matrix allowing local targeting of α particles

The localization of radium-223 dichloride particles within osteoblastic tumor was studied by autoradiography in mice sacrificed at 24, 48 and 72 h after single i.v. administration of radium-223. In mice intratibially inoculated with LuCaP 58 cells, a vast majority of radium-223 deposits was observed within the bone matrix and especially in the vicinity of activated osteoblasts. In addition, a few radium-223 deposits co-localized with prostate cancer cells (Fig. 5A). The mean value for total activity (gamma counts per minute) was higher in tumor-bearing tibiae compared to control non-tumored tibiae at 24 and 48 h (Fig. 5B; 24 h, $p = 0.00590$; 48 h, $p = 0.00332$).

A single radium-223 injection induces immediate effects on tumor cells, osteoblasts and osteoclasts in prostate cancer in bone

The immediate effects on tumors were studied after a single dose of radium-223 in LuCaP 58 tumor-bearing mice. Interestingly, radium-223 decreased serum PSA level in comparison to vehicle control ($p = 0.04926$) at 72 h post injection (Fig. 5C). Furthermore, there was a trend for increased relative necrotic tumor area in tumor-bearing tibia over time, although significance was not reached (Fig. 5D). The effect of radium-223 on inducing DNA double-strand breaks was evaluated by immunohistochemical staining of γ-H2AX molecules in LuCaP 58 tumor-bearing tibiae (14). DNA double-strand breaks were increased in tumor cells at all time points ($p = 0.00297$, 0.03665 and 0.00714 for 24, 48 and 72 h, respectively) and in osteoblasts and osteoclasts at 72 h after dosing ($p = 0.03148$ and 0.00071, respectively), compared to vehicle-treated mice at 72 h (Fig. 5E–G).

Discussion

Metastasis to bone has detrimental effects on bone, quality of life and survival (20, 21). While currently used palliative therapies for bone metastases in CRPC, such as zoledronic acid and the RANK-L inhibitor denosumab, are capable of reducing SREs and provide pain palliation (22–25), the targeted α-therapy radium-223 is the first drug with proven beneficial effect on overall survival (10). However, it has not been yet investigated in detail whether the beneficial clinical effects in prostate cancer patients are solely due to radium-223 affecting osteoblasts and/or osteoclasts, or if the treatment also has a direct effect on prostate cancer cells. Our results from preclinical studies with two different prostate cancer xenograft models, LNCaP representing osteoblastic/mixed lesions and LuCaP 58 PDX representing

osteoblastic lesions, demonstrate marked tumor growth suppression, and inhibition of tumor-induced bone alteration in radium-223-treated animals. We have previously reported similar findings with radium-223 treatment in a mouse model of osteolytic breast cancer bone metastasis (12), indicating that radium-223 is effective regardless of the primary tumor origin and the type of tumor-induced pathological effects on bone. In addition to the distinct tumor-induced reactions in bone, the observed differences in certain parameters may derive from the use of different mouse strains and distinct properties of the tumor cells. LNCaP is a cell line–derived model whereas LuCaP 58 model represents a patient-derived xenograft model. Furthermore, LuCaP 58 tumors grow very aggressively in comparison to LNCaP tumors, resulting in extra-osseous tumor growth and consecutively increased total tissue area.

Radium-223 uptake was recently characterized in healthy mice as well as in osteoblastic (LNCaP) and osteolytic (PC3) prostate cancer-bearing animals (26). This study showed that bone, specifically the areas of active bone remodeling and vascular supply, is the main target site for radium-223 accumulation. In mice with prostate cancer growing in bone, radium-223 accumulated on the bone surface next to the malignant site (26). Here, we assessed radium-223 deposition pattern in LuCaP 58 model representing a very strong osteoblastic component and demonstrated the efficient deposition of radium-223 into the intratumoral bone matrix, with the most substantial occurrence in the proximity of activated osteoblasts. A portion of radium-223 deposits was found in the midst of prostate cancer cells. The deposition pattern was in agreement with the increased uptake measured using gamma counter. However, the extent and nature of co-localization with tumor cells remains to be elucidated. The localization of radium-223 to the bone microenvironment adjacent to tumor, combined with the short track length of α-ray (2–10 cell diameters, < 100 μm), effectively limits the damage only to adjacent cells. This is further substantiated by high tolerability in mice and a low rate of hematological side effects in clinical trials with radium-223 (27–30).

Radium-223 induced DNA double-strand breaks in tumor cells 24, 48 and 72 h after dosing in mice bearing LuCaP 58 tumors. In addition, serum PSA level compared to vehicle control was decreased already at 72 h post treatment, indicating that the induction of DNA double-strand breaks is associated with significant tumor cell death. Furthermore, clear tumor necrosis was observed in tumor-bearing tibiae treated with radium-223. The observed radium-223 deposition pattern, together with its early effects on tumor cells, osteoblasts and osteoclasts, suggests direct and potent radiation effects on both tumor and bone cells in osseous tumor growth.

In addition to bone metastases, prostate cancer also causes visceral metastases to soft tissue in approximately 20% of patients participating in first-line studies for CRPC (31–33). Additional preclinical studies are necessary to investigate the possible roles and mode-of-action of radium-223 in inhibiting overall metastatic spread. The ability of radium-223 to trigger tumor cell death and to prevent both osteolytic and osteoblastic metastasis progression in the bone as well as secondary metastases to soft tissues concurrently would render this agent a very powerful therapy in the treatment of diverse solid tumors.

The observed decreases in both overall tumor burden as measured by PSA and in pathological bone changes as determined using the bone formation marker PINP in response to radium-223 treatment are in line with changes in PSA and alkaline phosphatase (ALP) observed in clinical setting (18, 19). Our preclinical data also suggest a dependency between decreased osteoblastic activity and decreased tumor burden in radium-223 treated mice as measured by various parameters reflecting pathological bone formation and tumor growth, respectively. Future studies with larger treatment groups are needed to determine if there is an association between ALP and response to radium-223.

There are currently multiple therapies with very distinct mechanisms of actions and unique toxicities available for the treatment of CRPC (5, 10, 31–38). Regrettably, clinical application has revealed that a large number of patients acquire resistance to most therapies after a short period of treatment and moreover, multiple patients exhibit *de novo* resistance. Of note, our data, similarly to clinical situation show that radium-223 is active in abiraterone-resistant prostate cancer, excluding the unlikely possibility that abiraterone resistance impairs the efficacy of radium-223. Resistance has not been described in association with α-therapy. However, the impact of genetic alterations, such as mutations in or copy-number variation of DNA repair mechanism genes, on the antitumor efficacy of radium-223 treatment in preclinical and clinical studies needs to be elucidated. For example, publicly available genomic data in LNCaP cells reveals several defects in DNA repair genes, such as *ATM* and *BRCA2* (39).

Radium-223 was recently shown to induce T cell-mediated lysis in human prostate, breast, and lung carcinoma cells (40). In our study with preclinical CRPC models established in immunocompromized mice, the host immune response and potential immunotherapeutic role of radium-223 in prostate cancer could not be addressed. Additional preclinical studies using immunocompetent mice will be useful in evaluating the immunotherapeutic effects of radium-223 in prostate cancer and the efficacy of radium-223 in combination with immune checkpoint inhibitors, such as PD-(L)1 inhibitors. Clinical evaluation of this is currently ongoing in a Phase I study evaluating the safety and tolerability of radium-223 in combination with atezolizumab (NCT02814669).

Taken together, our results indicate that radium-223 therapy exhibits a dual targeting mode-of-action that inhibits disease progression via tightly localized cytotoxic effects on tumor cells and stabilization of the bone microenvironment in bone metastases (Fig. 6). Based on clinical findings, our previously published results (12) and the data presented here, the potential of radium-223 in delaying time to SREs and bone metastases in patients with earlier phase of prostate cancer and also in patients with bone metastases from other solid tumors need to be evaluated. The focus of investigation is now on developing optimal combinations of the new therapeutic agents to effectively target the primary tumor as well as prevent metastasis to bone, resulting in increased survival and lower patient morbidity. Preliminary data from a post-hoc study exhibited improved overall survival in patients treated with radium-223 and concomitant abiraterone, enzalutamide, or denosumab, raising positive expectations for further research (30).

Supplementary Material

Refer to Web version on PubMed Central for supplementary material.

Acknowledgments

Financial support: The establishment of the LuCaP 58 PDX was supported by grants from the National Institutes of Health (E. Corey, National Institutes of Health, NIH PO1 CA085859 and NIH P50 CA097186). Bayer AG has paid Pharmatest Services Ltd. for the execution of the experiments. Editorial support was funded by Bayer AG.

We thank Natalia Habilainen-Kirillov, Riikka Kytömaa, Anniina Luostarinen, Johanna Rantanen, and Jani Seppänen for their skillful technical assistance. Aurexel Life Sciences Ltd. (www.aurexel.com) is acknowledged for the editorial support funded by Bayer AG. The establishment of the LuCaP 58 PDX was supported by grants from the National Institutes of Health (NIH PO1 CA085859 and NIH P50 CA097186).

References

1. Torre LA, Bray F, Siegel RL, Ferlay J, Lortet-Tieulent J, Jemal A. Global cancer statistics, 2012. CA Cancer J Clin. 2015; 65:87–108. [PubMed: 25651787]
2. Vignani F, Bertaglia V, Buttigliero C, Tucci M, Scagliotti GV, Di Maio M. Skeletal metastases and impact of anticancer and bone-targeted agents in patients with castration-resistant prostate cancer. Cancer Treat Rev. 2016; 44:61–73. [PubMed: 26907461]
3. Broder MS, Gutierrez B, Cherepanov D, Linhares Y. Burden of skeletal-related events in prostate cancer: unmet need in pain improvement. Support Care Cancer. 2015; 23:237–47. [PubMed: 25270847]
4. Jayasekera J, Onukwugha E, Bikov K, Mullins CD, Seal B, Hussain A. The economic burden of skeletal-related events among elderly men with metastatic prostate cancer. Pharmacoeconomics. 2014; 32:173–91. [PubMed: 24435407]
5. Fizazi K, Scher HI, Miller K, Basch E, Sternberg CN, Cella D, et al. Effect of enzalutamide on time to first skeletal-related event, pain, and quality of life in men with castration-resistant prostate cancer: results from the randomised, phase 3 AFFIRM trial. Lancet Oncol. 2014; 15:1147–56. [PubMed: 25104109]
6. Logothetis CJ, Basch E, Molina A, Fizazi K, North SA, Chi KN, et al. Effect of abiraterone acetate and prednisone compared with placebo and prednisone on pain control and skeletal-related events in patients with metastatic castration-resistant prostate cancer: exploratory analysis of data from the COU-AA-301 randomised trial. Lancet Oncol. 2012; 13:1210–7. [PubMed: 23142059]
7. Todenhofer T, Stenzl A, Hofbauer LC, Rachner TD. Targeting bone metabolism in patients with advanced prostate cancer: current options and controversies. Int J Endocrinol. 2015; 2015:838202. [PubMed: 25802521]
8. Loriot Y, Miller K, Sternberg CN, Fizazi K, De Bono JS, Chowdhury S, et al. Effect of enzalutamide on health-related quality of life, pain, and skeletal-related events in asymptomatic and minimally symptomatic, chemotherapy-naive patients with metastatic castration-resistant prostate cancer (PREVAIL): results from a randomised, phase 3 trial. Lancet Oncol. 2015; 16:509–21. [PubMed: 25888263]
9. Iuliani M, Pantano F, Buttigliero C, Fioramonti M, Bertaglia V, Vincenzi B, et al. Biological and clinical effects of abiraterone on anti-resorptive and anabolic activity in bone microenvironment. Oncotarget. 2015; 6:12520–8. [PubMed: 25904051]
10. Parker C, Nilsson S, Heinrich D, Helle SI, O'Sullivan JM, Fossa SD, et al. Alpha emitter radium-223 and survival in metastatic prostate cancer. N Engl J Med. 2013; 369:213–23. [PubMed: 23863050]
11. Sartor O, Coleman R, Nilsson S, Heinrich D, Helle SI, O'Sullivan JM, et al. Effect of radium-223 dichloride on symptomatic skeletal events in patients with castration-resistant prostate cancer and bone metastases: results from a phase 3, double-blind, randomised trial. Lancet Oncol. 2014; 15:738–46. [PubMed: 24836273]

12. Suominen MI, Rissanen JP, Kakonen R, Fagerlund KM, Alhoniemi E, Mumberg D, et al. Survival benefit with radium-223 dichloride in a mouse model of breast cancer bone metastasis. J Natl Cancer Inst. 2013; 105:908–16. [PubMed: 23682134]
13. Corey E, Quinn JE, Bladou F, Brown LG, Roudier MP, Brown JM, et al. Establishment and characterization of osseous prostate cancer models: intra-tibial injection of human prostate cancer cells. Prostate. 2002; 52:20–33. [PubMed: 11992617]
14. Redon CE, Nakamura AJ, Sordet O, Dickey JS, Gouliaeva K, Tabb B, et al. gamma-H2AX detection in peripheral blood lymphocytes, splenocytes, bone marrow, xenografts, and skin. Methods Mol Biol. 2011; 682:249–70. [PubMed: 21057933]
15. R Core Team. R: A language and environment for statistical computing. R Foundation for Statistical Computing; 2016. Available from: https://www.r-project.org/
16. Pinheiro, J., Bates, D., DebRoy, S., Sarkar, D., Team, RC. nlme: Linear and Nonlinear Mixed Effects Models. 2016.
17. Hothorn T, Bretz F, Westfall P. Simultaneous Inference in General Parametric Models. Biometrical Journal. 2008; 50:346–63. [PubMed: 18481363]
18. De Vincentis G, Follacchio GA, Frantellizzi V, Liberatore M, Monteleone F, Cortesi E. Prostate-Specific Antigen Flare Phenomenon During 223Ra-Dichloride Treatment for Bone Metastatic Castration-Resistant Prostate Cancer: A Case Report. Clin Genitourin Cancer. 2016; 14:e529–e33. [PubMed: 27212044]
19. McNamara MA, George DJ. Pain, PSA flare, and bone scan response in a patient with metastatic castration-resistant prostate cancer treated with radium-223, a case report. BMC Cancer. 2015; 15:371. [PubMed: 25948240]
20. Chen YC, Sosnoski DM, Mastro AM. Breast cancer metastasis to the bone: mechanisms of bone loss. Breast Cancer Res. 2010; 12:215. [PubMed: 21176175]
21. Clezardin P. Therapeutic targets for bone metastases in breast cancer. Breast Cancer Res. 2011; 13:207. [PubMed: 21586099]
22. Saad F, Gleason DM, Murray R, Tchekmedyian S, Venner P, Lacombe L, et al. A randomized, placebo-controlled trial of zoledronic acid in patients with hormone-refractory metastatic prostate carcinoma. J Natl Cancer Inst. 2002; 94:1458–68. [PubMed: 12359855]
23. Saad F, Gleason DM, Murray R, Tchekmedyian S, Venner P, Lacombe L, et al. Long-term efficacy of zoledronic acid for the prevention of skeletal complications in patients with metastatic hormone-refractory prostate cancer. J Natl Cancer Inst. 2004; 96:879–82. [PubMed: 15173273]
24. Fizazi K, Carducci M, Smith M, Damiao R, Brown J, Karsh L, et al. Denosumab versus zoledronic acid for treatment of bone metastases in men with castration-resistant prostate cancer: a randomised, double-blind study. Lancet. 2011; 377:813–22. [PubMed: 21353695]
25. Smith MR, Coleman RE, Klotz L, Pittman K, Milecki P, Ng S, et al. Denosumab for the prevention of skeletal complications in metastatic castration-resistant prostate cancer: comparison of skeletal-related events and symptomatic skeletal events. Ann Oncol. 2015; 26:368–74. [PubMed: 25425475]
26. Abou DS, Ulmert D, Doucet M, Hobbs RF, Riddle RC, Thorek DL. Whole-Body and Microenvironmental Localization of Radium-223 in Naive and Mouse Models of Prostate Cancer Metastasis. J Natl Cancer Inst. 2016:108.
27. Hoskin P, Sartor O, O'Sullivan JM, Johannessen DC, Helle SI, Logue J, et al. Efficacy and safety of radium-223 dichloride in patients with castration-resistant prostate cancer and symptomatic bone metastases, with or without previous docetaxel use: a prespecified subgroup analysis from the randomised, double-blind, phase 3 ALSYMPCA trial. Lancet Oncol. 2014; 15:1397–406. [PubMed: 25439694]
28. Nilsson S, Franzen L, Parker C, Tyrrell C, Blom R, Tennvall J, et al. Two-year survival follow-up of the randomized, double-blind, placebo-controlled phase II study of radium-223 chloride in patients with castration-resistant prostate cancer and bone metastases. Clin Genitourin Cancer. 2013; 11:20–6. [PubMed: 23021204]
29. Parker C, Finkelstein SE, Michalski JM, O'Sullivan JM, Bruland O, Vogelzang NJ, et al. Efficacy and Safety of Radium-223 Dichloride in Symptomatic Castration-resistant Prostate Cancer

Patients With or Without Baseline Opioid Use From the Phase 3 ALSYMPCA Trial. Eur Urol. 2016

30. Saad F, Carles J, Gillessen S, Heidenreich A, Heinrich D, Gratt J, et al. Radium-223 and concomitant therapies in patients with metastatic castration-resistant prostate cancer: an international, early access, open-label, single-arm phase 3b trial. Lancet Oncol. 2016; 17:1306–16. [PubMed: 27473888]
31. Petrylak DP, Tangen CM, Hussain MH, Lara PN Jr, Jones JA, Taplin ME, et al. Docetaxel and estramustine compared with mitoxantrone and prednisone for advanced refractory prostate cancer. N Engl J Med. 2004; 351:1513–20. [PubMed: 15470214]
32. Tannock IF, de Wit R, Berry WR, Horti J, Pluzanska A, Chi KN, et al. Docetaxel plus prednisone or mitoxantrone plus prednisone for advanced prostate cancer. N Engl J Med. 2004; 351:1502–12. [PubMed: 15470213]
33. Scher HI, Fizazi K, Saad F, Taplin ME, Sternberg CN, Miller K, et al. Increased survival with enzalutamide in prostate cancer after chemotherapy. N Engl J Med. 2012; 367:1187–97. [PubMed: 22894553]
34. de Bono JS, Oudard S, Ozguroglu M, Hansen S, Machiels JP, Kocak I, et al. Prednisone plus cabazitaxel or mitoxantrone for metastatic castration-resistant prostate cancer progressing after docetaxel treatment: a randomised open-label trial. Lancet. 2010; 376:1147–54. [PubMed: 20888992]
35. Fizazi K, Scher HI, Molina A, Logothetis CJ, Chi KN, Jones RJ, et al. Abiraterone acetate for treatment of metastatic castration-resistant prostate cancer: final overall survival analysis of the COU-AA-301 randomised, double-blind, placebo-controlled phase 3 study. Lancet Oncol. 2012; 13:983–92. [PubMed: 22995653]
36. Higano CS, Schellhammer PF, Small EJ, Burch PA, Nemunaitis J, Yuh L, et al. Integrated data from 2 randomized, double-blind, placebo-controlled, phase 3 trials of active cellular immunotherapy with sipuleucel-T in advanced prostate cancer. Cancer. 2009; 115:3670–9. [PubMed: 19536890]
37. Ryan CJ, Smith MR, Fizazi K, Saad F, Mulders PF, Sternberg CN, et al. Abiraterone acetate plus prednisone versus placebo plus prednisone in chemotherapy-naive men with metastatic castration-resistant prostate cancer (COU-AA-302): final overall survival analysis of a randomised, double-blind, placebo-controlled phase 3 study. Lancet Oncol. 2015; 16:152–60. [PubMed: 25601341]
38. Small EJ, Schellhammer PF, Higano CS, Redfern CH, Nemunaitis JJ, Valone FH, et al. Placebo-controlled phase III trial of immunologic therapy with sipuleucel-T (APC8015) in patients with metastatic, asymptomatic hormone refractory prostate cancer. J Clin Oncol. 2006; 24:3089–94. [PubMed: 16809734]
39. Forbes SA, Beare D, Gunasekaran P, Leung K, Bindal N, Boutselakis H, et al. COSMIC: exploring the world's knowledge of somatic mutations in human cancer. Nucleic Acids Res. 2015; 43:D805–11. [PubMed: 25355519]
40. Malamas AS, Gameiro SR, Knudson KM, Hodge JW. Sublethal exposure to alpha radiation (223Ra dichloride) enhances various carcinomas' sensitivity to lysis by antigen-specific cytotoxic T lymphocytes through calreticulin-mediated immunogenic modulation. Oncotarget. 2016; 7:86937–47. [PubMed: 27893426]

Translational significance

Radium-223 dichloride (Xofigo®) is a targeted alpha therapy demonstrating improved overall survival in CRPC patients with bone metastases. All the mechanisms-of-action of radium-223 in prostate cancer bone metastasis still remains to be completely understood. This study indicates that radium-223 therapy possesses a dual mode-of-action that inhibits tumor growth and suppresses tumor-induced abnormal bone formation, both essential players in the destructive vicious cycle of osteoblastic bone metastasis in prostate cancer. Our findings define the mechanisms by which radium-223 confers its observed clinical benefits and demonstrate the antitumor efficacy of radium-223 in an abiraterone-resistant patient-derived prostate cancer model with osseous tumor growth. These and our previously published data in a breast cancer bone metastasis model provide biological basis for developing new combinations and sequential treatment strategies for patients with prostate and potentially other solid cancers with bone metastases. Clinical studies on these additional cancer types are currently ongoing.

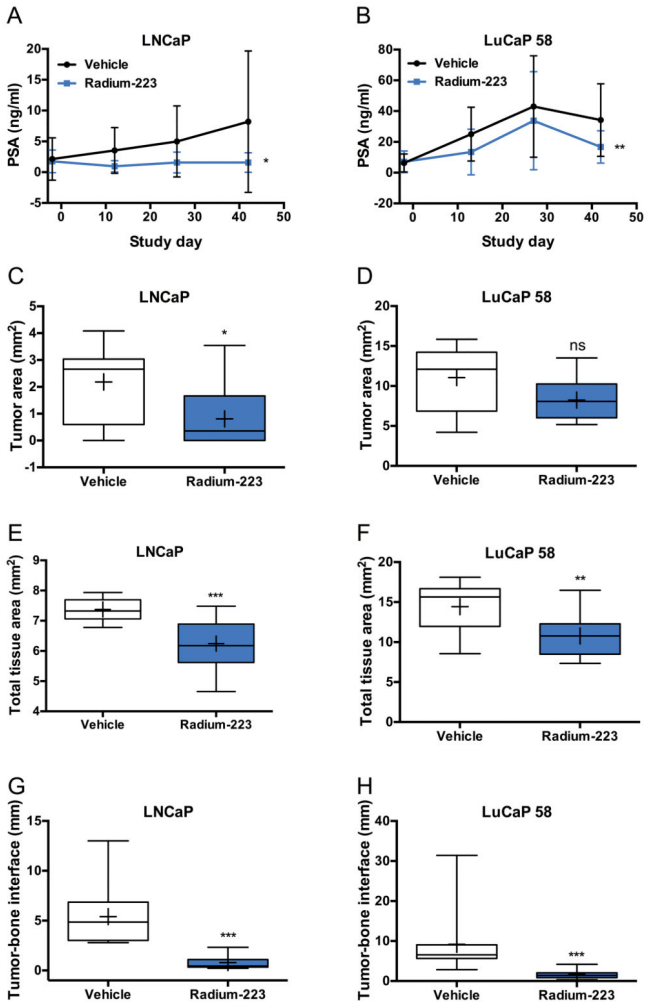

Figure 1. Radium-223 suppresses LNCaP and LuCaP 58 prostate cancer growth in bone in mouse models

A, Serum PSA levels in mice bearing LNCaP tumors, measured biweekly during dosing (mean ± SD, n = 10–14, p = 0.02771). **B,** Serum PSA levels in mice bearing LuCaP 58 PDX tumors, measured biweekly during dosing (mean ± SD, n = 16–18, p = 0.00191). **C,** Tumor area in mice bearing LNCaP tumors (n = 12–13, p = 0.00928). **D,** Tumor area in mice bearing LuCaP 58 tumors (n = 11, p = 0.09817). **E,** Total tissue area in mice bearing LNCaP tumors (n = 7–10, p = 0.91945). **F,** Total tissue area in mice bearing LuCaP 58 tumors (n = 11, p = 0.0697). **G,** The length of tumor-bone interface in mice bearing LNCaP tumors (n = 6–10, p = 0.00122). **H,** The length of tumor-bone interface in mice bearing LuCaP 58 tumors (n = 8–11, p = 0.00014). In box plots, horizontal lines show 5^{th}, 25^{th}, 50^{th}, 75^{th} and 95^{th} centiles and crosses indicate mean values. ns = not significant,* $p < 0.05$, ** $p < 0.01$, *** $p < 0.001$.

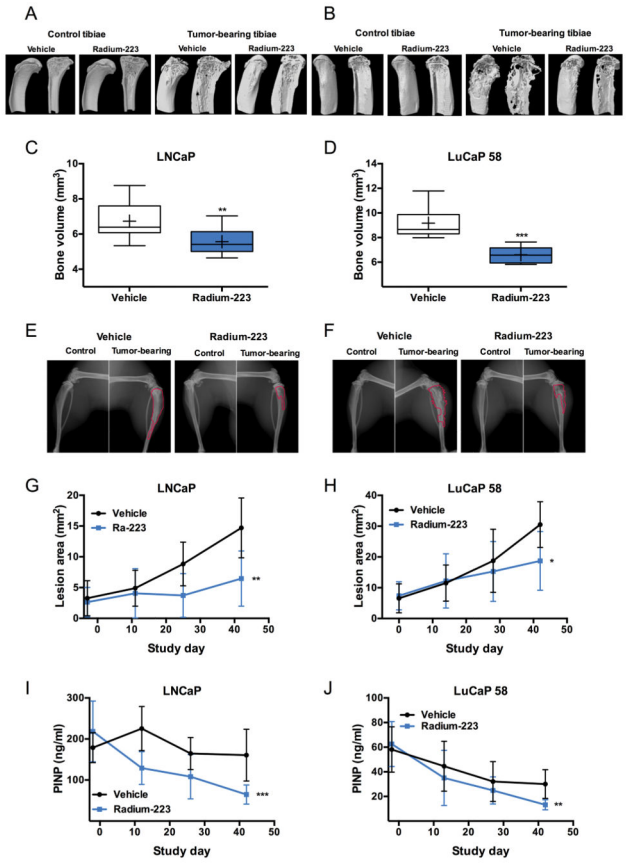

Figure 2. Radium-223 inhibits tumor-induced osteoblastic reaction resulting from LNCaP and LuCaP 58 prostate cancer growth in bone in mice

A–B, Representative micro-CT reconstructions of healthy and tumor-bearing tibias in (**A)** LNCaP and **(B)** LuCaP 58 models imaged from the medial side (measurement area starting 0.5 mm below the growth plate). Respective sagittal sections are shown on the right. Bone volume of tibias in mice bearing **C,** LNCaP (n = 12–13, p = 0.00450) or **D,** LuCaP 58 (n = 8–10, p < 0.001) tumors. In box plots, horizontal lines show 5th, 25th, 50th, 75th and 95th centiles and crosses indicate mean values. Representative radiographs of healthy and tumor-bearing tibias in (**E**) LNCaP and (**F**) LuCaP 58 models. Red line delineates the osteoblastic/osteolytic/mixed lesion area. Osteoblastic/mixed lesion area measured biweekly during dosing in mice bearing (**G**) LNCaP tumors (mean ± SD, n = 13, p = 0.00366) and (**H**) LuCaP 58 tumors (mean ± SD, n = 11–17, p = 0.01702). **I,** PINP levels in mice bearing LNCaP tumors were measured biweekly (mean ± SD, n = 13, p<0.001). **J,** PINP levels in mice bearing LuCaP 58 tumors were measured biweekly (mean ± SD, n = 11–15, p = 0.00548). * p<0.05, ** p<0.01, *** p<0.001.

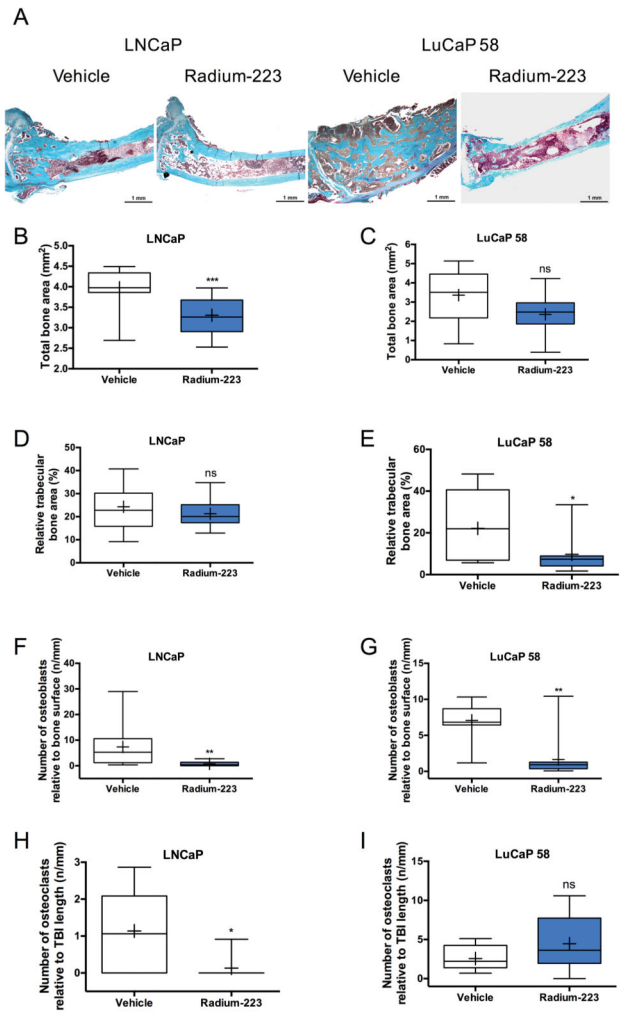

Figure 3. Radium-223 suppresses pathological bone formation in LNCaP and LuCaP 58 models of prostate cancer growth in mice

A, Representative MGT staining of bone architecture and tumor area in LNCaP and LuCaP 58 tumor-bearing mice treated with vehicle or Radium-223 (300 kBq/kg, i.v.). Turquoise indicates bone, pale pink tumor and dark pink bone marrow. Scale bar = 1 mm; 25x magnification. **B,** Total bone area in mice bearing LNCaP tumors (n = 12–13, p = 0.00059). **C,** Total bone area in mice bearing LuCaP 58 tumors (n = 11, p = 0.05883). **D,** Trabecular bone area relative to bone marrow area in mice bearing LNCaP tumors (n = 12–13, p = 0.43710). **E,** Trabecular bone area relative to bone marrow area in mice bearing LuCaP 58 tumors. (n = 11, p = 0.0212). **F,** The number of osteoblasts relative to bone surface in mice bearing LNCaP tumors (n = 12–13, p = 0.00127). **G,** The number of osteoblasts relative to bone surface in mice bearing LuCaP 58 tumors (n = 11, p = 0.0014). **H,** The number of osteoclasts relative to tumor-bone interface (TBI) in mice bearing LNCaP tumors (n = 6–10, p = 0.01207). **I,** The number of osteoclasts relative to TBI in mice bearing LuCaP 58 tumors (p = 8–11, 0.19644). In box plots, horizontal lines show 5^{th}, 25^{th}, 50^{th}, 75^{th} and 95^{th} centiles and crosses indicate mean values. ns = not significant,* p<0.05, ** p<0.01, *** p<0.001.

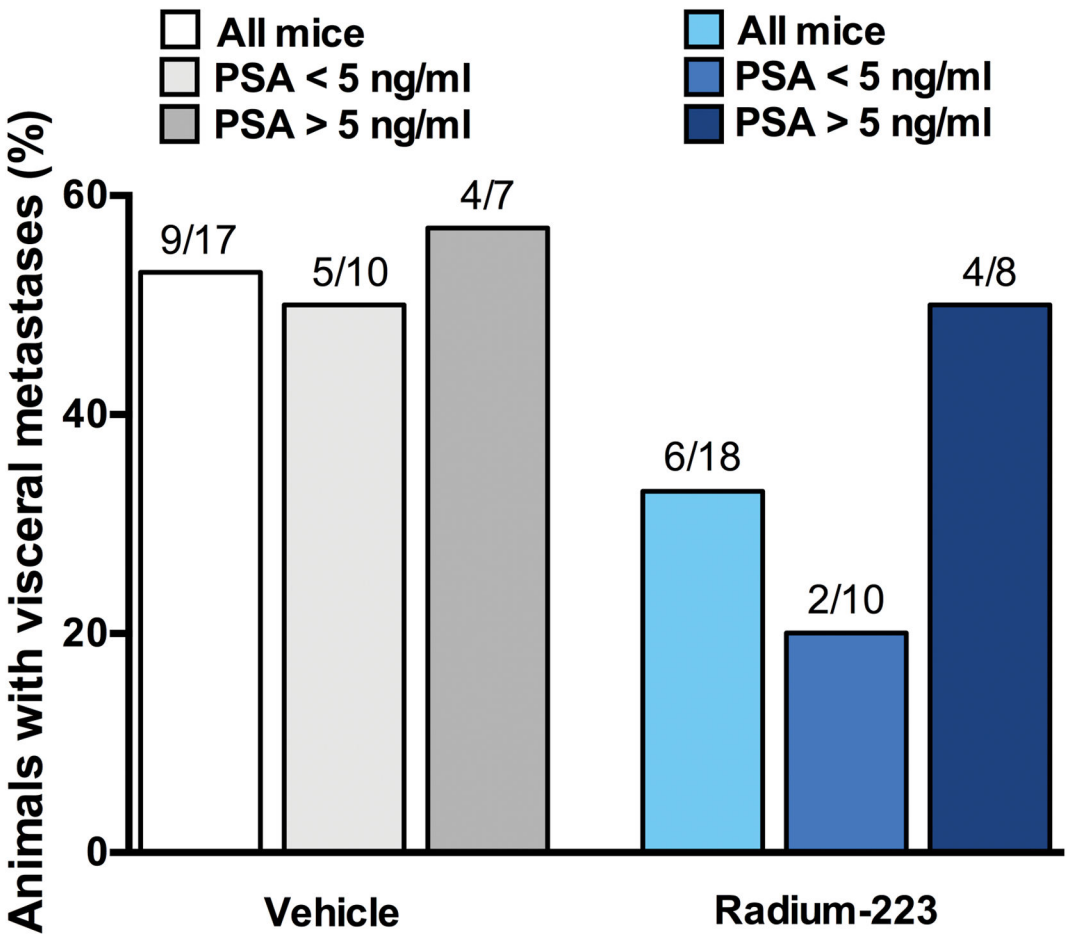

Figure 4. The effect of radium-223 treatment on visceral metastases in LuCaP 58 prostate cancer PDX model in mice

The number of mice with visceral metastases in mice treated with 28 mmol/L sodium citrate as vehicle or with radium-223 (300 kBq/kg, i.v.). The bars represent all mice, mice with smaller (PSA < 5 ng/mL) and mice with larger (PSA > 5 ng/mL) amount of tumor growth. The numbers above the bars represent the number of mice with visceral metastasis per the number of mice in a respective group.

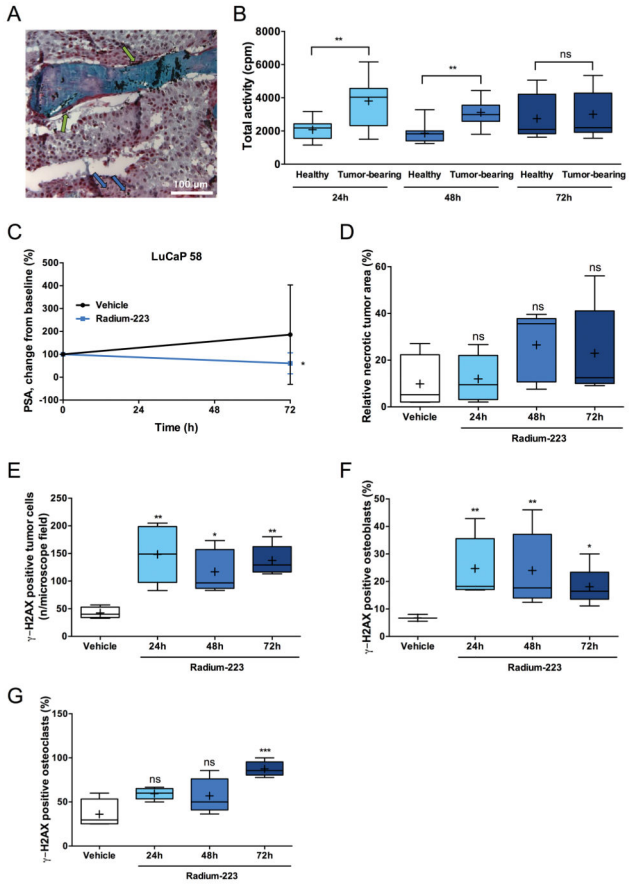

Figure 5. Radium-223 is deposited in the intratumoral bone matrix and induces DNA double-strand breaks in tumor cells, osteoblasts and osteoclasts in LuCaP 58 mouse model of prostate cancer growth in bone

A, Autoradiography analysis of undecalcified tissue sections was used to define the localization of radium-223 particles (black dots) in osteoblastic/mixed bone metastasis. Analysis was done at 24 h after single intravenous administration of radium-223 (300 kBq/kg). Green arrows indicate radium-223 deposition in the proximity of osteoblasts and blue arrows point radium-223 deposits within the tumor bed. Scale bar = 100 μm; 200x magnification. **B,** Total activity of healthy and contralateral tumor-bearing tibias of mice treated with single dose of radium-223 measured with a gamma counter (cpm, counts per minute; n = 11–12). **C,** Relative serum PSA 72 h after radium-223 dosing (% of value on day 0; mean ± SD, n = 11–12, p = 0.04926). **D,** Relative necrotic tumor area in animals sacrificed 24, 48, or 72 h after a single dose of radium-223 and 72 h after vehicle dosing (n = 4–5, p = 0.27134). **E,** γ-H2AX positive tumor cells (n/microscope field). The animals were sacrificed 24, 48, or 72 h after a single radium-223 dose and 72 h after vehicle dosing (n = 4–5; p = 0.00297, 0.03665 and 0.00714 for 24h, 48h and 72 h, respectively. **F,** γ-H2AX positive osteoblasts (% of all osteoblasts). The animals were sacrificed 24, 48, or 72 h after a single radium-223 dose and 72 h after vehicle dosing (n = 3–5; p = 0.03148 for 72h). **G,** γ-H2AX positive osteoclasts (% of all osteoclasts). The animals were sacrificed 24, 48, or 72 h after a single radium-223 dose and 72 h after vehicle dosing (n = 4–5; p = 0.00714 for 72h).

In box plots, horizontal lines show 5^{th}, 25^{th}, 50^{th}, 75^{th} and 95^{th} centiles and crosses indicate mean values. ns = not significant,* $p<0.05$, ** $p<0.01$, *** $p<0.001$.

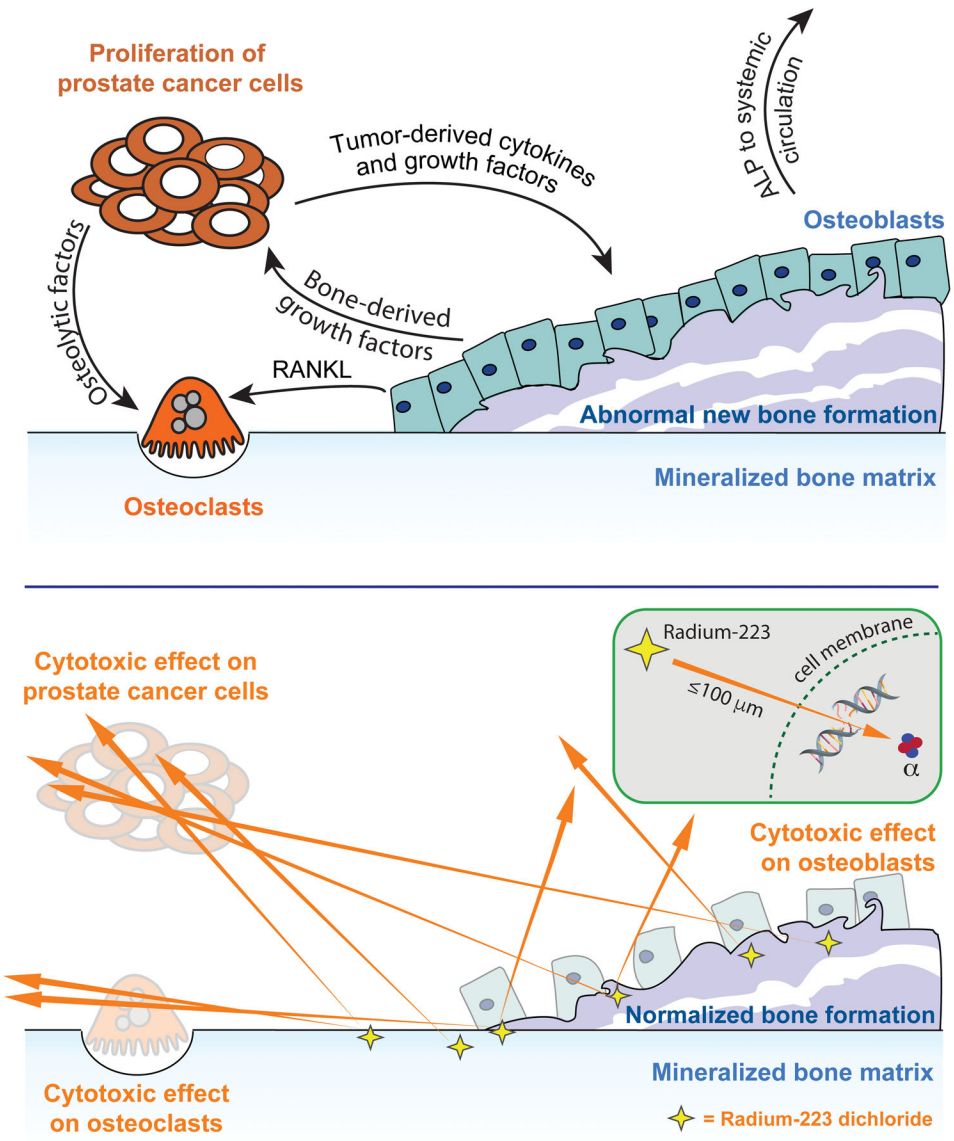

Figure 6. Radium-223 therapy exhibits a dual targeting mode-of-action that destroys tumor cells and inhibits tumor-induced pathological bone reaction

A, Tumor-induced dysregulation of bone remodeling is a key driver in prostate cancer-derived bone metastases. Prostate cancer bone metastases are commonly associated with abnormal osteoblastic bone growth. Prostate cancer cells release paracrine factors that affect both osteoblastic and osteoclastic activity and stimulate abnormal bone remodeling. Osteoblasts, in turn, secrete factors that promote progression of the prostate cancer metastases and stimulate osteoclast activity. The growth factors released from bone by activated osteoclasts further stimulate tumor growth. This complex vicious cycle of prostate cancer bone metastasis results in increased tumor growth and altered bone structure stability resulting eventually in bone destruction. RANKL, receptor activator of nuclear factor kappa-B ligand. **B,** Radium-223 is a targeted α-therapy with a dual targeting mode-of-action. Radium-223 inhibits the vicious cycle of prostate cancer bone metastases by inducing tightly

localized cytotoxic effects through double-stranded DNA breaks in osteoblasts, osteoclasts and prostate cancer cells.